**LETTER**

# I-V curve of the electron flow generated during a pyroelectric effect in lithium tantalate single crystal in vacuum conditions

View the article online for updates and enhancements.

# I-V curve of the electron flow generated during a pyroelectric effect in lithium tantalate single crystal in vacuum conditions

A. N. Oleinik[1(a)], M. E. Gilts[1], P. V. Karataev[2], A. A. Klenin[1] [iD], A. S. Kubankin[1,3] and P. G. Shapovalov[4]

[1] *Laboratory of Radiation Physics - Belgorod, Russia*
[2] *John Adams Institute at Royal Holloway, University of London - Egham, TW20 0EX, UK*
[3] *Lebedev Physical Institute - Moscow, Russia*
[4] *National Research Nuclear University "MEPhI" - Moscow, Russia*

**Abstract** – Realization of a pyroelectric effect in vacuum provides the possibility to develop a compact and relatively inexpensive electron source. In this paper we observe and analyze the I-V curve of electron flow generated during the pyroelectric effect in a lithium tantalate single crystal. The region of the monoenergetic electron flow with a slow change in the peak energy is determined. This phenomenon is accompanied by a current avalanche process. The analysis of the electron spectra and the I-V curve shows that the observed avalanche process and the stabilization of the peak energy occurs due to a sharp increase of secondary electrons in the total electron flow.

**Introduction.** – Electrification of dielectrics in vacuum can be used to generate a high electric field of up to $10^6$ V/cm [1]. The electrification of materials with spontaneous polarization is an area of particular interest, because the electric field can be generated by an external mechanical or thermal influence known as the piezoelectric or the pyroelectric effect, respectively [1,2]. The high electric field leads to a so-called field electron emission either from the charged surface or from the surrounding conductors depending on the sign of the induced charge [3]. This phenomenon underlies the pyroelectric and piezoelectric accelerator concepts. In these devices, electrons are accelerated to the energy of the order of several tens of keV [4,5]. Such type of accelerator can be used to generate X-rays, neutrons, positive ions, as well as to control charged particle beams. On the other hand, it is considered as a cheap and simple instrument for operation under non-standard conditions [6–13].

The emitted electrons have two remarkable properties: the flow is self-focused at a certain distance from the emission plane [12] and is monoenergetic with slowly changing value of energy. The latter phenomenon is not fully understood. Simultaneous measurement of current and voltage makes it possible to obtain the *V-I* dependence, which is

widely used to describe the properties of devices and structures under test [14,15]. However, it is very difficult to measure the potential difference between the pyroelectric material and the target directly. We found two indirect ways to evaluate the potential. The first way is to determine the endpoint energy of the X-ray spectrum, which cannot be higher than the potential difference [16]. However, the accuracy of this method depends on the position of the X-ray detector and the X-ray flux intensity. The second way is a direct measurement of the electron flux, where the peak is observed and its position defines the potential difference [1,4].

Both ways are implemented in this work to determine the *I-V* curve of the electron flow during the pyroelectric excitation of a lithium tantalate single crystal (LiTaO$_3$, LT), which has a large pyroelectric coefficient compared to other pyroelectric materials [17]. The periodic temperature variation is used to change the temperature of the crystal [18]. Standard geometry of the pyroelectric accelerator [10–13] is modified to measure the current and the electron spectrum simultaneously. Based on the analysis of the *I-V* curve and electron spectra, we can distinguish the primary electron flux of electrons emitted from the surface of the LT sample and the secondary electron flux, produced predominantly from the metallic target being irradiated. The avalanche process is associated with a sharp

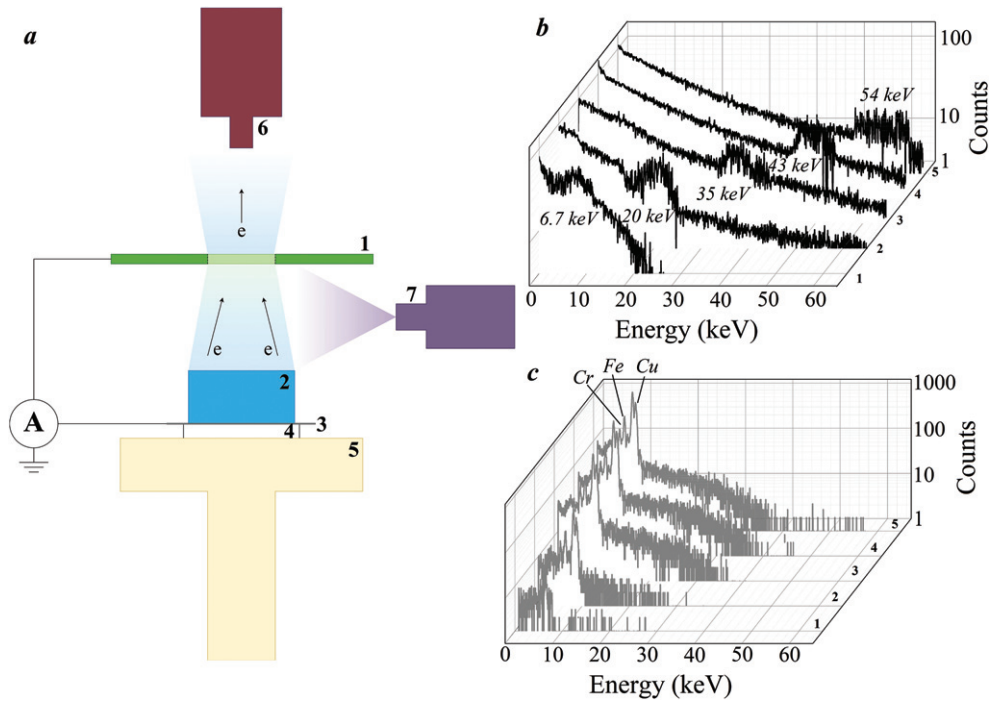[(a)]E-mail: oleynik_a@bsu.edu.ru (corresponding author)

Fig. 1: (a) Scheme of experiment. 1: brass target; 2: LiTaO$_3$ single crystal; 3: aluminum foil; 4: Peltier element; 5: aluminum heat sink; 6: electron detector; 7: X-ray detector. Evolution of the electron (b) and X-ray (c) spectra during a half-cycle of temperature variation at the negative polarity phase. Numbers in panels (b) and (c) correspond to numbers in fig. 2.

increase of the number of the secondary electrons and leads to the primary electron flux stabilization. However, the flux peak becomes less intense and broader during the avalanche process, which may indicate a distortion of the emitted electron flow.

**Experiment.** – The geometry of the pyroelectric accelerator is shown in fig. 1(a). The target was a brass plate 400 $\mu$m thick with a 0.3 mm hole. The target is mounted coaxially with the vertical axis passing through the center of the polar surface of LT single crystal (2). The crystal has a cylindrical shape (the $Z$-axis is co-directed with the cylinder guide) with a diameter of 20 mm and the height of 10 mm. The area of the target is much larger than the polar LT crystal surface. An aluminum foil (3), which served as the second electrode in the electric circuit was attached to the crystal with a conductive epoxy glue. The Peltier element (4) is used to apply the temperature changing in time. The reverse side of the Peltier element is glued to an aluminum heat sink (5) for efficient heat exchange. The electron detector Ortec CR-012-025-100 (6) was located 30 mm behind the target coaxially with the hole. The X-ray spectrometer Amptek Cd-Te X-123 (7) mounted through a side flange was used to measure X-ray emission from both the crystal and the target surfaces.

The target served as an electrode for closing the current measurement circuit. A part of the electrons passed through the hole and was registered by the detector. The measurement of the electron current was carried out by connecting the target and the foil

glued to the lower surface of the LT crystal into a circuit through the picoammeter Keithley 6485 [13]. The temperature of the pyroelectric material was changed in a sinusoidal mode [18] with the frequency of 0.5 mHz and the amplitude of 18 °C near the top crystal surface (the temperature changed between 20 °C and 38 °C). The typical vacuum level was varied from 0.05 to 50 mTorr. The vacuum level was controlled using the manual valve. The change occurs in the pause between the half-waves of the generated particles, *i.e.*, at the maximal or minimal temperature. During active particle generation, the pressure was almost constant. The vacuum control was provided by a fore vacuum (Geowell GWSP150) and a turbomolecular (Oerlikon TMP50) pumps. Here we present results obtained only during the negative polarity phase, when the negative charge is induced on the upper polar surface and emission occurs from the crystal.

**Results and discussion.** – Figures 1(b) and (c) present the evolution of the electron and X-ray spectra during a half-cycle of temperature variation at the negative polarity phase. The energy of the electron peak increases, but, at the same time, the peak amplitude decreases and the width increases. A sharp increase in the continuous background along with an increase in the peak energy is associated with growth of the secondary electron production. The X-ray spectrum contains the characteristic lines of copper and zinc from the brass target, iron and chromium lines from the vacuum chamber wall. The endpoint energy of the X-ray spectrum increases following the electron peak energy up to 35 keV. However, after
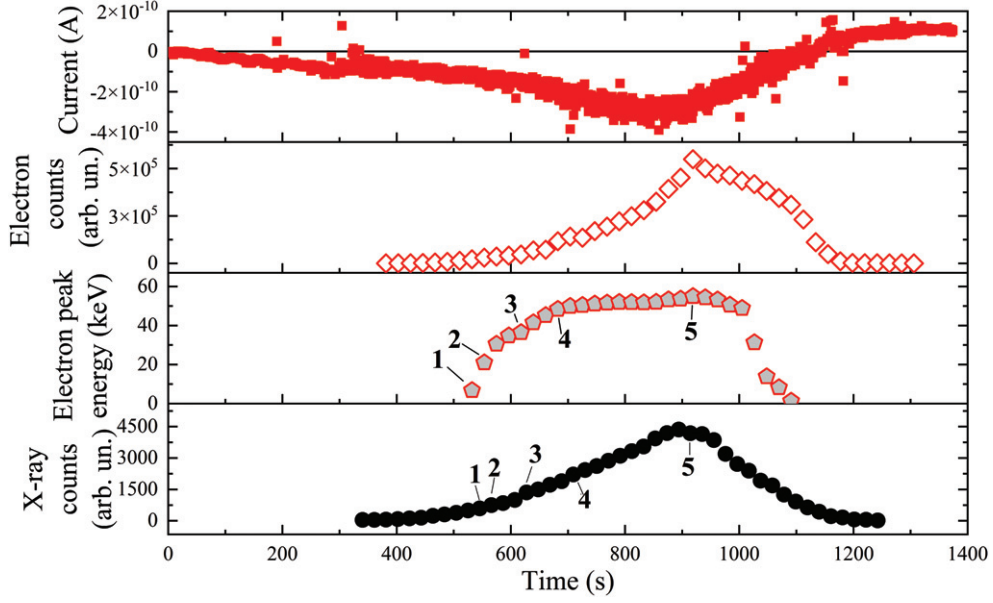
Fig. 2: The parameters of electron and X-ray fluxes during a half-cycle of temperature variation at a residual gas pressure of 1 mTorr. From top to bottom: electron current, number of counts in electron spectra, energy of electron peak, number of counts in X-ray spectra. The numbers correspond the numbers in fig. 1.
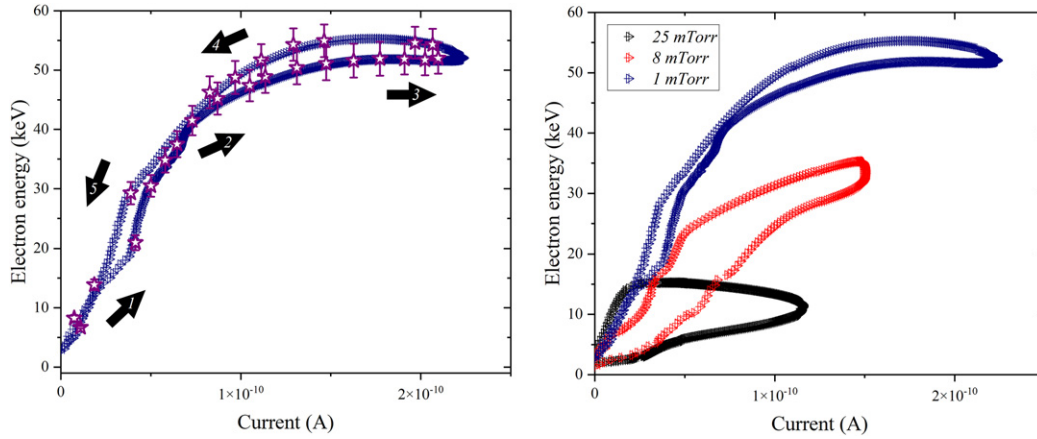


Fig. 3: (a) The *I-V* curve of the electron flux based on data from fig. 2. (b) *I-V* curve of the electron flux at different values of residual gas pressure. The course of the curve is shown by numbered arrows. For the curves in panel (b) it is similar.

that the endpoint energy saturates while the peak energy keeps on growing until it becomes noticeably higher. A small number of high-energy photons can be associated with a non-optimal position of the X-ray detector, when radiation emission from the target is observed at the acute angle of 3°. This is a demonstration that the electron peak energy monitoring is a more accurate way to determine the potential difference.

The electron and X-ray fluxes *vs.* time during a half-cycle of temperature variation and at residual gas pressure of 1 mTorr are shown in fig. 2. A sinusoidal electron current with the amplitude of about 115 pA is observed. An additional wave is superimposed on the second half of the sine function, so that the total current level reaches 400 pA. The additional and main wave go down together

until the current polarity reverses, *i.e.*, the transition to the positive polarity, when the electrons move from the target to the LT crystal. The maximal number of electron counts in the spectrum is observed a bit later than the maximum of the current curve. The peak of monoenergetic electrons in the spectrum appears closer to the maximum of the main current wave and disappears along with the change of polarity. The peak energy is stable during the additional current wave only. The numbers indicate the points corresponding to the spectra in fig. 1. Spectra 4 and 5 were taken during the additional electron wave with a slight difference in the peak position, which also indicates the stabilization of the particle generation process.

The *I-V* curve of the electron flux, based on the peak energy and electron current measurement (see fig. 2) is shown
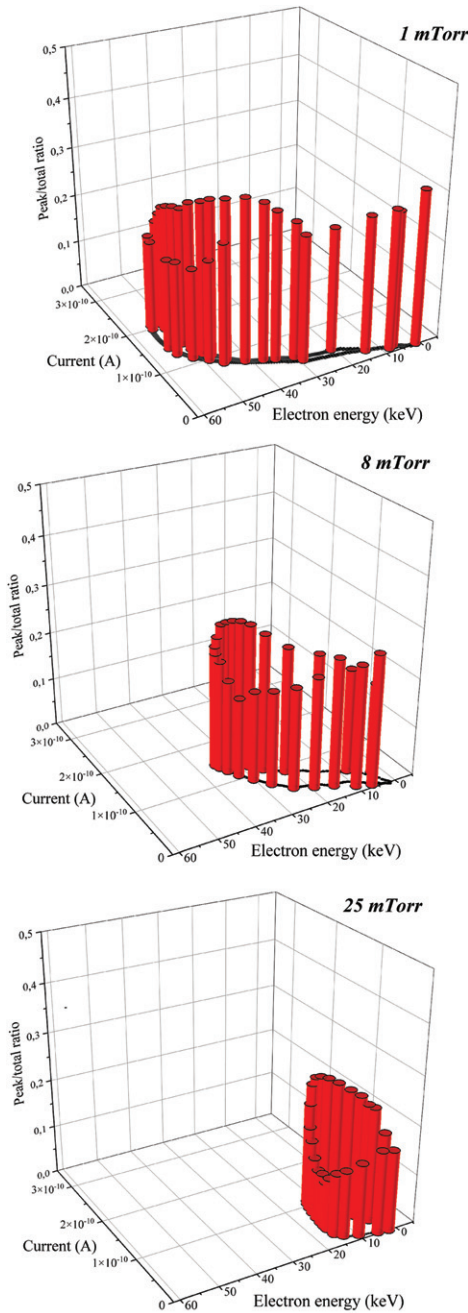
Fig. 4: The peak/total ratio for *I-V* curves from fig. 3.

distortion of the *I-V* curve and the weakening of the discharge. Therefore, the observed avalanche process is not the Townsend discharge.

The main contribution to the background of the electron spectrum comes from secondary electrons, including those that are kicked out of the target. The spectra presented in fig. 1, demonstrate a sharp increase in the secondary electron contribution. Previously, it was shown that one of the indicators of the stability of the pyroelectric accelerator is the peak/total ratio (the number of events in the peak to the total number of events in the spectrum [22]). Figure 4 presents the change of the peak/total ratio for all three *I-V* curves presented in fig. 3. First, the peak/total ratio first slowly increases during the sharp increase of the current (the start of the avalanche), and then drops down when the current reaches the maximum (the maximum of the avalanche). It should be noted that the growth of the peak/total ratio is much slower than the growth of the total number of events in the electron spectrum. Therefore, during the avalanche discharge and stabilization of the peak energy, the current growth occurs due to the impact ionization of the target material. Thus, we can assume that the avalanche discharge and the stabilization of the peak energy (and hence the stabilization of the potential difference) are observed due to the influence of the secondary electron emission from the target.

An increase in pressure leads to a gradual suppression of the flow of secondary electrons [23] and the reduction of the amplitude of the avalanche process. In turn, the energy of the monoenergetic electrons also decreases. As a result, the electron energy peak smears out and gradually disappears. The above effects cause the median value of the peak/total ratio to drop. Thus, the monoenergetic electron flow with a slow change in the energy might appear due to the secondary electrons, which cannot leave the region between the crystal and the target. These electrons take out a part of the power induced by the temperature change preventing further accumulation of the potential.

**Conclusion.** – Simultaneous measurement of the current and the electron spectrum in a pyroelectric accelerator allows to obtain the *I-V* curve. A remarkable detail of the *I-V* curve is a hysteresis loop with energy of the electron peak changing slowly. An additional wave is observed in the current providing evidence of the avalanche process. The shape of the curve is similar to the I-V curve of a non-self-sustaining Townsend discharge, however, the conditions for the avalanche initiation are principally different. The avalanche weakens when pressure level increases. The peak/total ratio [22] drops during the avalanche indicating that the main source of additional electrons is the target, but not the residual gas. An important fact is the observation of peak energy stabilization during the avalanche demonstrating their relationship. However, the peak itself becomes weaker and wider indicating that the monoenergetic electron flow is distorted.

in fig. 3(a). The additional wave forms a closed hysteresis loop with the peak energy changing by no more than 20% within 350 seconds. The observed *I-V* curve is very similar to the non-self-sustained Townsend discharge [19–21]. It allows us to assume that the observed additional wave is an avalanche process, and the stabilization of the peak energy is associated with this discharge. The *I-V* curve depends on the residual gas pressure as shown in fig. 3(b). The higher pressure increases the probability of impact ionization of the residual gas molecules, which is the main mechanism for initiation of the Townsend discharge [19]. However, in our case, an increase in pressure leads to a

The study of the avalanche process, the conditions for its occurrence and the possibilities of maintaining the primary electron flow with stable energy have become new goals in the study of the electron generation in the pyroelectric accelerator. The key influence of the secondary electron emission suggests that the target material with different secondary electron emission coefficient needs to be investigated. From a practical point of view, the correct selection of the target material provides the possibility to regulate the long-term monoenergetic phase of the electron flow, which, of course, is a driver for the development of practical devices based on the concept of the pyroelectric accelerator.

$$* * *$$

*Data availability statement*: The data that support the findings of this study are available upon reasonable request from the authors.

REFERENCES

[1] BROWNRIDGE J. D., *Electron and positive ion beams and x-rays produced by heated and cooled pyroelectric crystals such as LiNbO₃ and LiTaO₃ in dilute gases: phenomenology and applications*, in *Trends in Electro-Optics Research* (Nova Science Publishers, New York) 2005, pp. 57–74, ISBN:978-1594544989.

[2] TAGANTSEV A., *Sov. Phys. Usp.*, **30** (1987) 588.

[3] ROSENMAN G. *et al.*, *J. Appl. Phys.*, **88** (2000) 6109.

[4] GEUTHER J. A. and DANON Y., *J. Appl. Phys.*, **97** (2005) 074109.

[5] IVASHCHUK O. O. *et al.*, *Sci. Rep.*, **8** (2018) 16488.

[6] GEUTHER J. A. and DANON Y., *J. Appl. Phys.*, **97** (2005) 10491.

[7] NARANJO B., GIMZEWSKI J. and PUTTERMAN S., *Nature*, **434** (2005) 1115.

[8] GEUTHER J. A., DANON Y. and SAGLIME F., *Phys. Rev. Lett.*, **96** (2006) 54803.

[9] OLEINIK A. N. *et al.*, *JINST*, **11** (2016) P08007.

[10] WILKE M. *et al.*, *J. Vac. Sci. Technol. B*, **37** (2019) 011203.

[11] GHADERI R. and DAVANI F. A., *Appl. Phys. Lett.*, **106** (2015) 042906.

[12] BROWNRIDGE J. D. and SHAFROTH S. M., *Appl. Phys. Lett.*, **79** (2001) 3364.

[13] BROWNRIDGE J. D. *et al.*, *Appl. Phys. Lett.*, **78** (2001) 1158.

[14] HUO W., ZHOU H. and DU C., *EPL*, **139** (2022) 56002.

[15] JOACHIM C. and GIMZEWSKI J. K., *Europhys. Lett.*, **30** (1995) 409.

[16] OLEINIK A. N. *et al.*, *Bull. Lebedev Phys. Inst.*, **48** (2021) 127.

[17] GEUTHER J. A., *Radiation generation with pyroelectric crystals*, PhD Thesis, Rensselaer Polytechnic Institute (2007), URL: `https://hdl.handle.net/20.500.13015/3836`.

[18] OLEINIK A. N. *et al.*, *J. Appl. Phys.*, **132** (2022) 204101.

[19] MASSINES F. *et al.*, *Plasma Phys. Control. Fusion*, **47** (2005) B577.

[20] XIAO D., *Fundamental Theory of Townsend Discharge* (Springer) 2016, ISBN:978-3-662-48041-0.

[21] LUO H., WANG X. and LI C., *EPL*, **97** (2012) 15002.

[22] KARATAEV P. *et al.*, *Appl. Phys. Express*, **15** (2022) 066001.

[23] ARUMUGAM S. *et al.*, *Curr. Smart Mater.*, **2** (2017) 44.